

# Quantifying the influence of sill intrusion on the thermal evolution of organic-rich sedimentary rocks in nonvolcanic passive margins: an example from ODP 210-1276, offshore Newfoundland, Canada

Alexander Peace,\* Ken McCaffrey,\* Jonathan Imber,\* Richard Hobbs,\* Jeroen van Hunen\* and Keith Gerdes†

\*Department of Earth Sciences, Durham University, Durham, UK

†Shell International Exploration and Production, Den Haag, The Netherlands

## ABSTRACT

Intrusive magmatism is an integral and understudied component in both volcanic and nonvolcanic passive margins. Here, we investigate the thermal effects of widespread (*ca.* 20 000 km<sup>2</sup>) intrusive magmatism on the thermal evolution of organic-rich sedimentary rocks on the nonvolcanic Newfoundland passive margin. ODP 210-1276 (45.41°N, 44.79°W) intersects two sills: an older, upper sill and a younger, lower sill that are believed to correspond to the high amplitude ‘U-reflector’ observed across the Newfoundland Basin. A compilation of previous work collectively provides; (1) emplacement depth constraints, (2) vitrinite reflectance data and (3) <sup>40</sup>Ar/<sup>39</sup>Ar dates. Collectively, these data sets provide a unique opportunity to model the conductive cooling of the sills and how they affect thermal maturity of the sedimentary sequence. A finite differences method was used to model the cooling of the sills, with the model outputs then being entered into the EASY%R<sub>o</sub> vitrinite reflectance model. The modelled maturation profile for ODP 210-1276 shows a significant but localized effect on sediment maturity as a result of the intrusions. Our results suggest that even on nonvolcanic margins, intrusive magmatism can significantly influence the thermal evolution in the vicinity of igneous intrusions. In addition, the presence of widespread sills on nonvolcanic passive margins such as offshore Newfoundland may be indicative of regional-scale thermal perturbations that should be considered in source rock maturation studies.

## INTRODUCTION

Continental extension causes rifting and thinning of the lithosphere that may result in continental breakup and eventually the initiation of seafloor spreading (Eldholm & Sundvor, 1979). Passive continental margins are a product of this continental breakup and subsequent seafloor spreading (Geoffroy, 2005). Passive margins are traditionally classified as one of two end-member types: (1) volcanic (VPM) or (2) nonvolcanic (NVPM), in reference to the relative abundance or scarcity of igneous rocks produced during rifting and breakup (e.g. Franke, 2013).

Passive margins globally represent a significant host for both current (e.g. offshore Newfoundland; DeSilva, 1999) and future hydrocarbon exploration targets (e.g. offshore West Africa; Beglinger *et al.*, 2012). Source rock quality, and in particular maturity, is of paramount concern when exploring new areas in deep water passive margins where operating costs may be high. To reduce the exploration risk in these settings, it is thus important to

understand and quantify the thermal evolution of NVPMs, and their source rock maturation characteristics. Syn and post-rift magmatism is a common feature on passive margins, with spatially extensive igneous sill complexes being a common feature on both volcanic (e.g. the Western Australian margin; Holford *et al.*, 2013) and nonvolcanic passive margins (e.g. the South Australian Margin; Holford *et al.*, 2012). The heat from these intrusions may contribute to the thermal evolution of a margin, and thus the maturation of potential source rock material. It is for this reason that the additional heat introduced by igneous intrusions into prospective sedimentary basins on passive margins needs to be quantified.

ODP 210-1276 intersects two sills which provide an opportunity to model potential changes in the maturity of the encasing organic-rich sedimentary host rocks instigated by post-rift magmatism in a NVPM. Here, we report the results of 1D conductive modelling of the influence of sill intrusion and compare the model predictions with the measured vitrinite reflectance data of Pross *et al.* (2007) to estimate the maturation state of the encasing sedimentary rocks. Experiments were also undertaken to understand the roles of timing, hydrothermalism

Correspondence: Alexander Peace, Department of Earth Sciences, Durham University, Durham DH1 3LE, UK.  
E-mail: a.l.peace@durham.ac.uk

and the duration in which sills acted as magmatic conduits.

The aim of this work was to show that despite all the variables present in a complex intrusive system such as this, a simple model can be used to account for the majority of thermal effects. This allows us to discount less important processes, resulting in insights into the major controls on the thermal maturation of organic-rich sedimentary rocks in proximity to igneous intrusions. We conclude that the sills intersected at ODP 210-1276 have influenced the localized thermal evolution of the sedimentary rocks, which may be indicative of a broader, more regional thermal perturbation in the region covered by the 'U-reflector'. Although, given that ODP 210-1276 essentially represents a 1D profile through a

spatially extensive, complex, igneous system, it is likely that the results presented herein are not representative of the situation in other parts of the Newfoundland Basin.

## GEOLOGICAL SETTING

The Newfoundland margin was formed during the opening of the North Atlantic and in conjunction with its conjugate, the Iberian margin, it is considered to be a typical NVPM (e.g. Melankholina, 2011; Peron-Pinvidic *et al.*, 2013). ODP site 210-1276 (45.41°N, 44.79°W) was drilled into transitional crust offshore Newfoundland, Canada (Fig. 1). The aim of this ODP

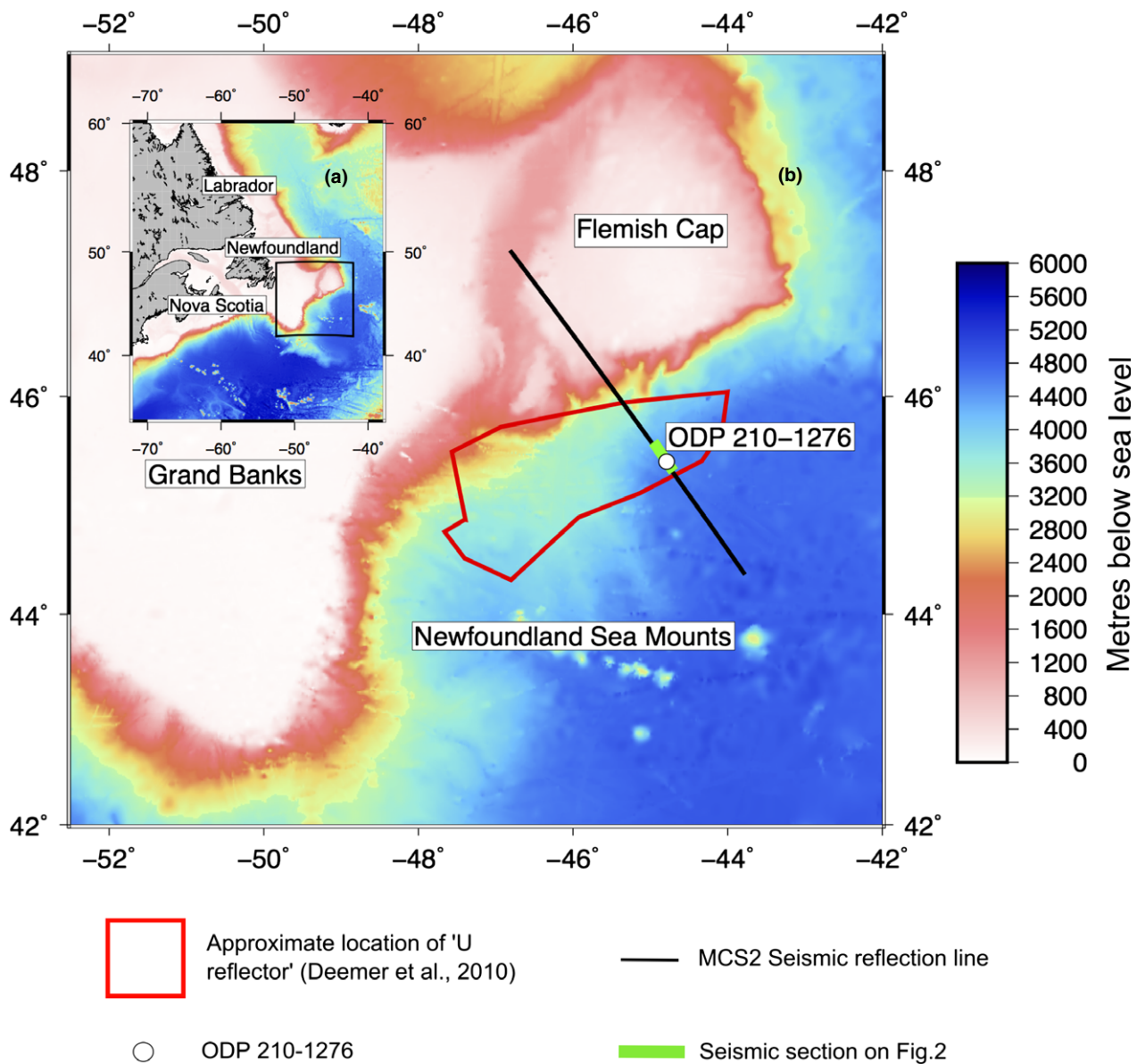


Fig. 1. (a) An overview of the Eastern Canadian continental margin. (b) The study area showing the location of ODP site 210-1276, along with seismic line MCS2 (section shown in Fig. 2 in green) and the approximate location of the 'U-reflector' (Deemer *et al.*, 2010). Bathymetry data produced from satellite altimetry by Smith & Sandwell (1997).

**Table 1.** Intrusion parameters of the sills at ODP 210–1276. Current positions in well (Tucholke *et al.*, 2004a), depth when intruded (Tucholke *et al.*, 2007) and  $^{40}\text{Ar}/^{39}\text{Ar}$  ages (Hart & Blusztajn, 2006)

Name	Current top of unit (mbsf)	Current bottom (mbsf)	Thickness (m)	Depth when intruded (mbsf)	Youngest $^{40}\text{Ar}/^{39}\text{Ar}$ Ar age (ma)	Oldest $^{40}\text{Ar}/^{39}\text{Ar}$ Ar age (ma)
Upper sill	1612.7	1623	10.30	ca. 260	$104.7 \pm 1.7$	$105.9 \pm 1.8$
Lower sill	1719	>1736.9	17.90	ca. 590	$95.9 \pm 2$	$99.7 \pm 1.8$

leg was to provide a greater understanding of the syn and post-rift stratigraphy and magmatic history of the conjugate Newfoundland-Iberia nonvolcanic passive margins (Tucholke *et al.*, 2004a), with the specific aim of targeting what was believed from seismic reflection data to be the breakup unconformity, which ultimately turned out to be igneous intrusions. The drill site is located near the edge of the thinned continental crust (Van Avendonk *et al.*, 2006), with the well encountering two intervals of igneous rocks which are modelled herein. These two intervals; are the only igneous rocks recorded at ODP 210–1276, consisting of an upper, singular sill which is 10.3 m thick and a lower sill complex where the main body is at least 17.9 m thick (Table 1). Drilling ceased 17.9 m after penetrating the main body of the lower sill, thus modelling a sill of this thickness represents a minimum and the thermal influence is likely to be greater. The first sill was emplaced after the onset of seafloor spreading (Peron-Pinvidic *et al.*, 2010), which was initiated by Barremian to Aptian time (anomaly M3 to M0, or 127–112 Ma) Hopper *et al.* (2004).

Previous work has associated the sills at this site with the widespread ‘U-reflector’ observed in 2D seismic reflection profiles (e.g. Fig. 2) across the Newfoundland basin (e.g. Shillington *et al.*, 2004; Deemer *et al.*, 2010). The U-reflector is considered to represent a suite of post-breakup magmatic intrusions covering an area of ca. 20 000 km<sup>2</sup> Deemer *et al.* (2010) in an otherwise nonvolcanic margin. It is observable on seismic reflection data as one or two high amplitude reflectors, at a depth corresponding to the igneous intrusions at ODP 210–1276. Within the resolution of the seismic reflection profile it is not possible to determine if the high amplitude reflectors correspond to singular or multiple igneous intrusions, but given the observed situation intersected by ODP 210–1276 it is likely that the high amplitude reflectors at this depth across the Newfoundland Basin represent at least one igneous intrusion.

The widespread nature of the sills on the Newfoundland margin (Deemer *et al.*, 2010) implies that this igneous activity represents a significant margin-scale event. In contrast, no significant post-rift intrusive activity is known on the conjugate Iberian margin, implying an asymmetric post-breakup magmatic history (Peron-Pinvidic *et al.*, 2010). The sills of the U-reflector are of interest due to their close proximity to the offshore Newfound-

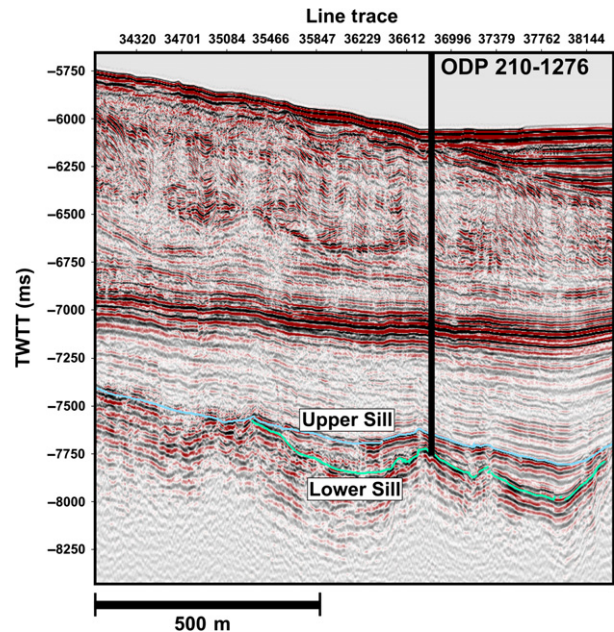


**Fig. 2.** Segment of MCS (multichannel seismic) reflection profile SCREECH 2 (Studies of Continental Rifting and Extension on the Eastern Canadian Shelf) by Shillington *et al.* (2004) where it intersects ODP site 210–1276. The location of this seismic line segment is shown on the study area overview map (Fig. 1b). Interpretation of the U-reflector (green/blue lines) from Peron-Pinvidic *et al.* (2010).

land petroleum systems. Karner & Shillington (2005) qualitatively suggested that these sills could have implications for the thermal history of the region.

Chronological analysis by Hart & Blusztajn (2006) of the sills at ODP 210–1276 provided  $^{40}\text{Ar}/^{39}\text{Ar}$  dates of  $104.7 \pm 1.7$  Ma and  $105.9 \pm 1.8$  Ma for the upper sill, and  $95.9 \pm 2$  Ma and  $99.7 \pm 1.8$  Ma for the lower sill (Table 1 and Fig. 3). The  $^{40}\text{Ar}/^{39}\text{Ar}$  dates demonstrate that there was a time interval of ca. 5–10 Myrs between the intrusions cooling to their closing temperatures. Compositionally, both sills are classified as alkali basalt – hawaiite (Hart & Blusztajn, 2006).

The sills are located within uppermost Aptian to lowermost Albian syn-rift sequences at ca. 90–160 m and ca. 200–270 m above basement for the upper and lower sills respectively. This is based on the interpretation of seismic reflection profiles, including the SCREECH MCS2 line which crosses ODP 210–1276 (Fig. 2), and calculated vertical seismic velocities which are;

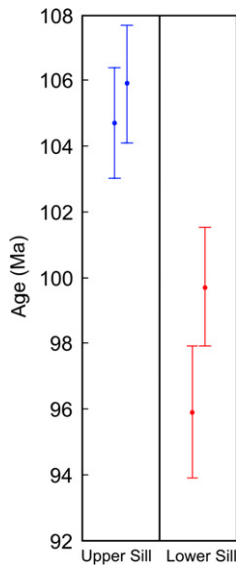


Fig. 3.  $^{40}\text{Ar}/^{39}\text{Ar}$  dates, and associated  $2\sigma$  errors for the upper and lower sills from Hart & Blusztajn (2006).

4738–5030  $\text{ms}^{-1}$ , 5527–6193  $\text{ms}^{-1}$  and 1650–3200  $\text{ms}^{-1}$  for the upper sill, lower sill and sediments between the sills, respectively, according to Tucholke *et al.* (2004b).

The sills were intruded at shallow depths of *ca.* 260 m and *ca.* 590 m into relatively unconsolidated, and not overpressured sedimentary rocks, particularly in the lower 30 m of the section (Tucholke *et al.*, 2007). This suggests that at the drill site the upper sill had considerable mechanical support probably provided by nearby dykes, protecting the underlying sedimentary rocks from compaction due to the load of the later sedimentary overburden (Peron-Pinvidic *et al.*, 2010). The emplacement depths were calculated by consideration of the  $^{40}\text{Ar}/^{39}\text{Ar}$  Ar dates in the context of the nano-fossil based age vs depth curve provided by Tucholke *et al.* (2004a). This age depth relationship was established using zonal boundary ages of microfossils at ODP 210–1276. Karner & Shillington (2005) used a reconstruction of porosity–depth relationships to estimate an intrusion depth of 0–556 m below sea floor. These two independent estimates do not account for any subsequent burial and compaction (Tucholke *et al.*, 2007).

The sedimentary rocks present at ODP 210–1276 include siltstones, sandstones, carbonates and shale-clast conglomerates (Fig. 4). Of most interest to this study are the organic-rich rocks found in several intervals in ODP 210–1276 (Fig. 4), as these could provide potential source material. Total Organic Carbon (TOC wt% – the amount of carbon bound in an organic compound) was collected between 801 and 1713 m below seafloor by Tucholke *et al.* (2004a). TOC values are recorded between 0 and 9.7 wt% at ODP 210–1276, with values in proximity to the intrusions <2 wt%. Pross *et al.* (2007) conducted a maturation study on the rocks in proximity to the upper sill describing them as predominantly dark grey mudrocks, with minor sand to silt-based turbidites and black shales (Fig. 4).

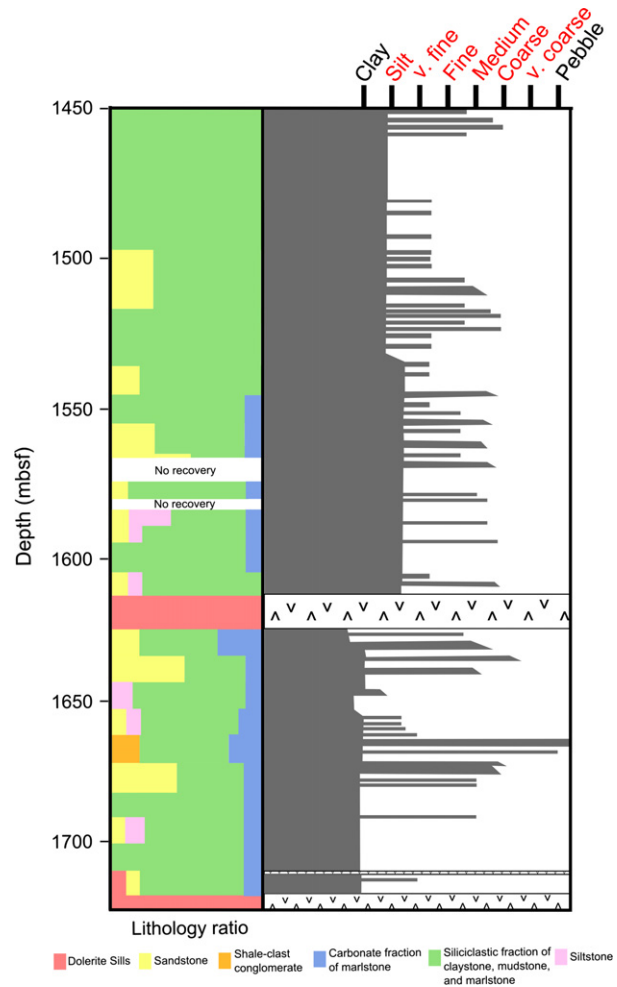


Fig. 4. Lithostratigraphic column and grain size reproduced from Tucholke *et al.* (2004a) for the interval of ODP 210–1276 in proximity to the sills, with depth in mbsf (metres below sea-floor). The organic-rich sedimentary rocks of interest to this study can be found in several intervals and are depicted in pink.

## METHODOLOGY

### Model setup

We performed numerical calculations to investigate the thermal influence of the igneous intrusions intersected at ODP 210–1276 on the surrounding sedimentary rocks. The temperatures obtained from one-dimensional finite difference MATLAB models were entered into the EASY%R<sub>0</sub> model of Sweeney & Burnham (1990) to produce theoretical vitrinite reflectance values.

Thermal heat diffusion was considered to be the dominant process affecting thermal evolution, and is described in the models by:

$$\frac{\partial T}{\partial t} = D \frac{\partial^2 T}{\partial x^2}, \quad (1)$$

where  $T$  is the Temperature,  $t$  is time,  $x$  is distance and  $D$  = the thermal diffusion coefficient:

$$D = \frac{k}{\rho C_p}, \quad (2)$$

where  $k$  = thermal conductivity,  $\rho$  = density and  $C_p$  = specific heat capacity.

The simplifications and assumptions made in our model include: (1) the only form of heat transfer is considered to be conduction; (2) latent heat released from crystallization of the sills is accounted for by the inclusion of a calculated higher starting temperature equivalent to an extra 488°C; (3) emplacement of the sills was instantaneous; (4) thermal parameters are not temperature dependent; (5) stratigraphical units are considered to be internally homogeneous; and (6) the regional geothermal gradient (Table 2) remained constant during margin evolution. The validity of these assumptions is discussed below.

- (1) Our models assume that heat transfer was by conduction only (e.g. Fjeldskaar *et al.*, 2008; Aarnes *et al.*, 2010; Wang *et al.*, 2010, 2007). Advective heat transport by hydrothermal activity is negligible in low permeability materials such as shales (Aarnes *et al.* (2010), although the stratigraphic sequence encountered in ODP 210-1276 (Fig. 4) is dominated by sandstones (Tucholke *et al.*, 2004a) with a higher permeability than shale. Therefore, additional heat advection due to heating and circulation of pore waters may lead to more rapid cooling than conduction alone, and our results may represent a minimum estimate of the cooling rate.
- (2) We approximate the latent heat effect of magma crystallization in our model by applying a starting

temperature of the sill that is increased with the released heat during magma crystallization: (3)

$$\Delta T_{\text{latent}} = \frac{L_{\text{intrusion}}}{C_{p \text{ intrusion}}}, \quad (3)$$

where  $\Delta T_{\text{latent}}$  is the additional heat from latent heat of crystallization,  $L_{\text{intrusion}}$  is the latent heat of crystallization (Spear & Peacock, 1989) and  $C_{p \text{ intrusion}}$  is the specific heat capacity of mafic intrusions (Barker *et al.*, 1998).

The sills are compositionally alkali basalt-hawaiite according to Hart & Blusztajn (2006). The initial temperature of the intrusion is therefore taken to be 1000°C; the same temperature as previous work modelling intrusions of similar composition (e.g. Barker *et al.*, 1998). Inclusion of latent heat of crystallization gives a modelled starting temperature of 1488°C, this includes 488°C additional heat from the latent heat of crystallization, on top of the initial temperature value of 1000°C for the sills as in Barker *et al.* (1998).

Latent heat has been omitted by some previous workers in this area of study (e.g. Barker *et al.*, 1998; Fjeldskaar *et al.*, 2008), whereas in others it has been included (e.g. Wang *et al.*, 2012). We choose to include latent heat in our models as it is a physical phenomenon, which could have a significant effect on the results. Although it has been noted by Galushkin (1997) that models accounting for latent heat could potentially over estimate its effects, as all the additional heat is added instantaneously rather than over the duration in which cooling occurs.

- (3) The main models presented herein assume instantaneous intrusion. This is a reasonable assumption

**Table 2.** Parameters utilized in the thermal modelling and symbols used in equations, excluding the EASY%R<sub>0</sub> parameters which are defined alongside the equations and in Table 3

Parameter	Symbol	Value	Units	Reference
Density of country rock	$\rho_{\text{host}}$	2400	kg m <sup>-3</sup>	Wang <i>et al.</i> (2012)
Density of intrusion	$\rho_{\text{intrusion}}$	2960	kg m <sup>-3</sup>	Wang <i>et al.</i> (2007)
Specific heat capacity of host	$C_{p \text{ host}}$	1090	J kg <sup>-1</sup> °C <sup>-1</sup>	Wang <i>et al.</i> (2012)
Specific heat capacity of intrusion	$C_{p \text{ intrusion}}$	820	J kg <sup>-1</sup> °C <sup>-1</sup>	Barker <i>et al.</i> (1998)
Conductivity of organic-rich host	$K_{\text{host}}$	2.1	W m <sup>-1</sup> °C <sup>-1</sup>	Wang <i>et al.</i> (2012)
Conductivity of intrusion	$K_{\text{intrusion}}$	2.5	W m <sup>-1</sup> °C <sup>-1</sup>	Wang <i>et al.</i> (2012)
Heat release from latent heat of crystallization	$\Delta T_{\text{latent}}$	488	°C	Calculated from $L_{\text{intrusion}}$ and $C_{p \text{ intrusion}}$ Equation 3
Diffusion coefficient	D	Varies spatially	m s <sup>-2</sup>	This work using Equation 2
Latent heat of crystallization	$L_{\text{intrusion}}$	400	kJ kg <sup>-1</sup>	Spear & Peacock (1989)
Geothermal gradient	G	21.75	°C km <sup>-1</sup>	Keen (1979)
Starting temperature of intrusion	$T_{\text{initial}}$	1000	°C	Barker <i>et al.</i> (1998)
Temperature at surface	$T_{\text{surf}}$	20	°C	This work
Spatial discretization step	$dx$	2	m	This work
Timestep	$dt$	0.1	years	This work
Distance between sills at time of intrusion	$H_{\text{past}}$	330	m	Tucholke <i>et al.</i> (2004a)
Current distance between sills	$H_{\text{current}}$	96	m	Tucholke <i>et al.</i> (2004a)
Current depth of upper sill top	$S_{\text{current}}$	260	m (below sea floor)	Tucholke <i>et al.</i> (2004a)
Upper sill top at time of intrusion	$S_{\text{past}}$	1612.7	m (below sea floor)	Tucholke <i>et al.</i> (2004a)
Compaction factor	C	29.09%	%	Calculated from $H_{\text{current}}$ and $H_{\text{past}}$
Burial	B	1353	m	Calculated from $S_{\text{current}}$ and $S_{\text{past}}$

because the periods of emplacement were probably very short, as multiple samples from the sills gave statistically similar  $^{40}\text{Ar}/^{39}\text{Ar}$  ages (Hart & Blusztajn, 2006). Noninstantaneous intrusion will reduce the thermal effects of the intrusion as multiple smaller bodies will cool faster, than a singular large body. Previous authors modelling the influence of sills on organic matter have also assumed intrusion to be instantaneous (e.g. Aarnes *et al.*, 2010). Considering emplacement to be instantaneous increases the thermal effects of the intrusions in the modelling, and thus may lead to an overestimate of the maturation of organic-rich sedimentary rocks.

- (4) Keeping the thermal parameters (specific heat capacity and thermal conductivity – Table 2) constant over a temperature range, simplifies the modelling and is an assumption made by most previous work (e.g. Fjeldskaar *et al.*, 2008). It should also be considered that reducing the variables allows us to study the main controls on maturation, particularly as this study has observed vitrinite reflectance data available to provide a constraint.
- (5) Our model incorporates spatial variability in the thermal parameters between the units, but the units are internally assumed to be homogeneous, with the host having the thermal properties of dry organic-rich

shale. It is assumed to be dry so that heat transfer occurs through conduction only. Two units are recognized in our model; (1) ‘host rock’ and (2) ‘sills’ (Table 2, Fig. 5). This is a simplification also made by previous work (e.g. Wang *et al.*, 2012) which utilized separate values of thermal conductivity, density and specific heat capacity for ‘wall rock’ and ‘magma’.

- (6) The background geothermal gradient used in the model is based upon calculations by Keen (1979) for the current geothermal gradient on other parts of the Eastern Canadian Margin ( $17.5^\circ\text{C km}^{-1}$  for the Scotian Margin and  $26^\circ\text{C km}^{-1}$  for the Labrador Shelf). Our model utilizes an average of these values of  $21.75^\circ\text{C km}^{-1}$  (Table 2) as the study area is located between the Scotian Margin and the Labrador Shelf. Goutorbe *et al.* (2007) produced a detailed analysis of heat flow along the Eastern Canadian margin from offshore Labrador to Nova Scotia finding, there was no significant variation between the different sub-areas on the margin and that the nature of the continental basement and the age of the ocean floor had little influence. The geothermal gradient can justifiably remain constant for the modelled period as it only represents 60, 000 years, and these sills were both emplaced post margin breakup.

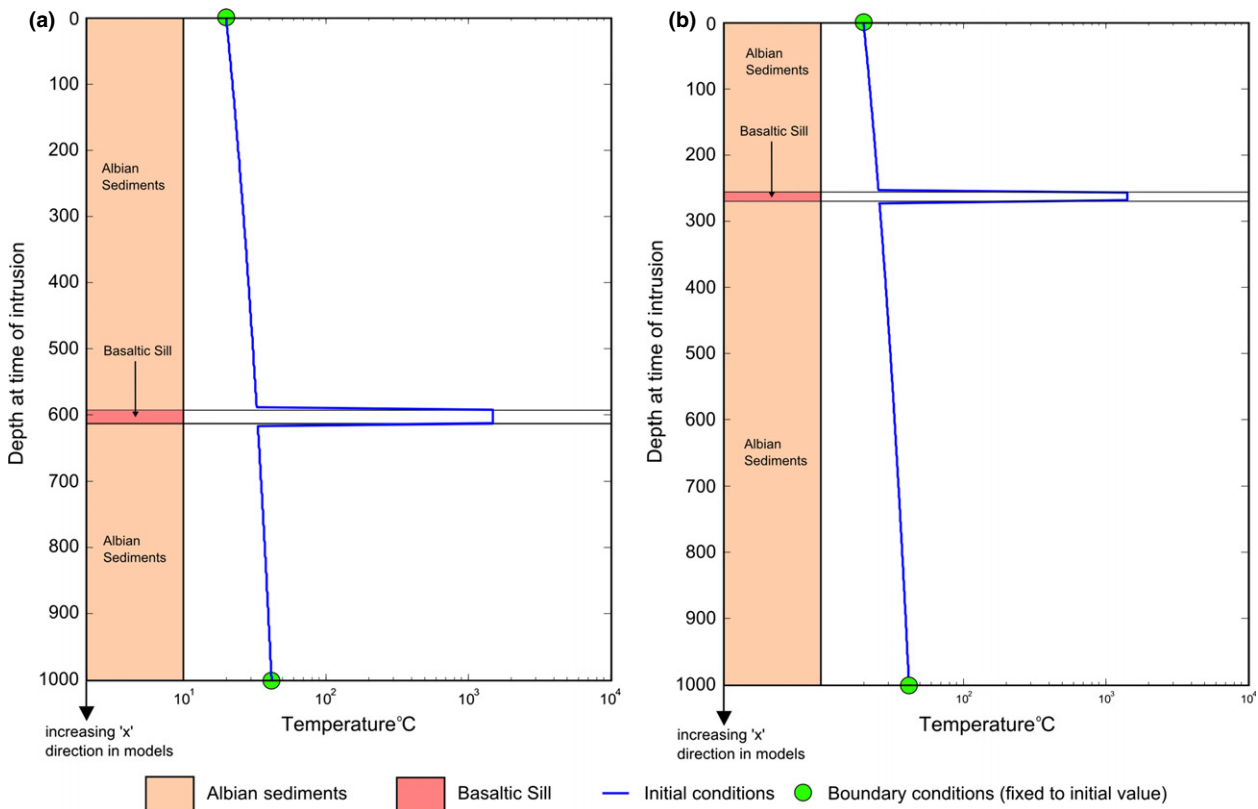


Fig. 5. Schematic depiction of the model setup for (a) the lower sill and (b) the upper sill. The initial temperature profile is depicted in blue for both (a) and (b). The boundaries are fixed and are shown in green. The relative positions of the two lithologies in (a) and (b) are shown. The parameters applicable to these lithologies can be found in Table 2. Model resolution ( $dx$ ) is 2 m and the time step ( $dt$ ) is 0.1 years. The X direction in the model is down hole.

The heat diffusion equation is solved in MATLAB with a finite differences method. Initial temperature conditions are shown in Fig. 5, and prescribed temperature boundary conditions equal the initial conditions. We model sills of 10 and 18 m thickness for which a vertical resolution of 2 m proved sufficient. Our discretization allows for spatial variation in thermal parameters.

The  $^{40}\text{Ar}/^{39}\text{Ar}$  ages provided by the previous work of Hart & Blusztajn (2006) record the closing temperatures, implying that these two cooling events were at least 1.5 Myrs apart (Fig. 3 and Table 1), a timescale that will be shown below to be much larger than the thermal equilibrium timescales of the sills. In our primary models we therefore consider the sills as individual thermal events rather than having occurred simultaneously. This is an improvement over previous models that consider multiple intrusions occur simultaneously (e.g. Fjeldskaar *et al.*, 2008), potentially overestimating the total heating event. The  $^{40}\text{Ar}/^{39}\text{Ar}$  dates provided by Hart & Blusztajn (2006) are highly statistically significant, with a *ca.* 7.5 Myrs difference using  $2\sigma$  uncertainties in measured age between the two sills. Comparison between the maximum temperatures achieved (and resulting maturation effects) when simultaneous intrusion is assumed was also modelled, and compared to the results of modelling the sills separately (Fig. 6).

As  $^{40}\text{Ar}/^{39}\text{Ar}$  ages of Hart & Blusztajn (2006), represent the time of cooling to closure temperature, they do not allow us to rule out if the sills acted as long-term conduits for magma. This is plausible in what appears on seismic reflection data to be a large, complex, intrusive system. If a sill acts for a large duration of time as a conduit for magmatism, then the thermal effect on the surrounding sediments will be increased when compared to an instantaneously intruded sill.

To provide a constraint on the duration in which a sill acted as a magmatic conduit we modelled systems in which the upper sill acted as a magma conduit for 10, 100 and 1000 years prior to cooling, quantifying the effects on theoretical vitrinite reflectance values produced using the EASY% $R_o$  of Sweeney & Burnham (1990). The modelled vitrinite reflectance values are then compared to the observed values of Pross *et al.* (2007), allowing estimations of the duration that the upper sill acted as a magmatic conduit to be constrained.

Emulating an open magmatic conduit is achieved by maintaining the sill at its starting temperature for the desired duration prior to cooling. In these models the sill has a starting temperature of 1000°C, with the additional 488°C contribution from the latent heat of crystallization added when the sill is allowed to cool. The magmatic conduit is assumed to be receiving a constant supply of magma, until it is allowed to cool.

During each model run the temperature at the boundaries was fixed to the initial conditions. Our discretization of the thermal diffusion equation (Equation 1 and 2) allows for spatial variation in thermal parameters. The model resolution ( $dx$ ) is 2 m and the timestep ( $dt$ ) is 0.1 years in all the models we ran. The values used for the parameters in equations 1, 2 and 3 are given in Table 2.

### Vitrinite reflectance modelling

Vitrinite reflectance (% $R_o$ ) is one of the most widely used indicators of source rock maturity. It is measured optically (Bostick & Alpern, 1977), and is useful in maturation studies as the degree of reflectivity varies smoothly and predictably with temperature (Burnham & Sweeney, 1989). However, there are several known drawbacks with the use of vitrinite reflectance as an indicator of organic sediment maturity (Heroux *et al.* (1979). These include

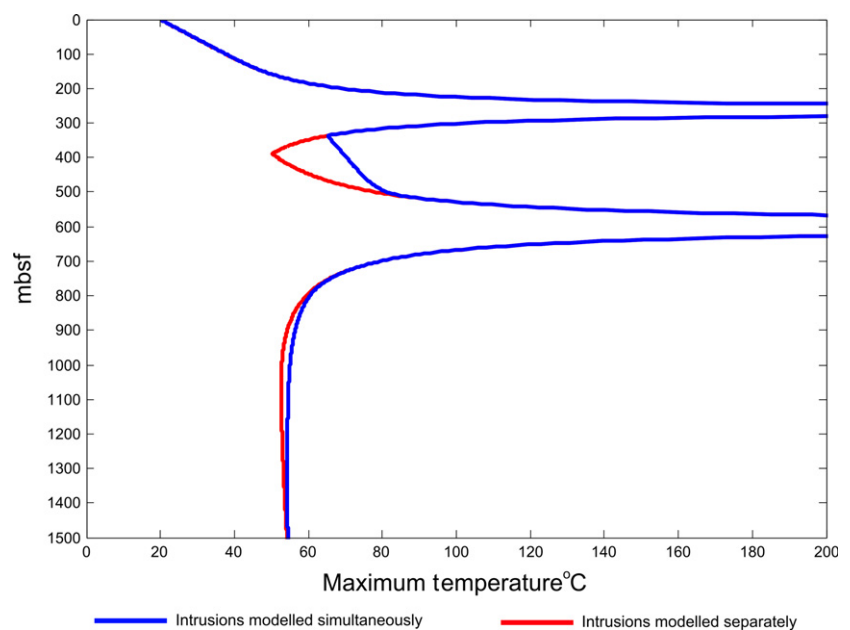


Fig. 6. Maximum temperatures achieved when the sills are modelled separately and simultaneously. All other figures depict the results from either a singular sill or models where the sills cooled separately, and the results subsequently combined.

but are not limited to, measurements being taken from similar known vitrinite minerals and the possible reworking of organic material.

This work utilizes the EASY%R<sub>o</sub> model of Sweeney & Burnham (1990), to calculate theoretical vitrinite reflectance values. EASY%R<sub>o</sub> calculates vitrinite reflection against time for a given stratigraphic level if the temperature–time history has been calculated, and can be used to produce a depth profile if multiple levels are calculated. It is a simplified version of the earlier VITRIMAT model of Burnham & Sweeney (1989), which is based on experimentally derived kinetic responses in a wide range of organic matter to account for the elimination of water, carbon dioxide, methane and higher hydrocarbons from vitrinite. The model is applicable over a wide range of vitrinite reflectance values (%R<sub>o</sub>), and heating rates.

EASY%R<sub>o</sub> is based on an Arrhenius first-order parallel reaction approach with a distribution of activation energies (Table 3), thus the reaction can be described as:

$$\frac{dw}{dt} = -kw, \quad (4)$$

where the reaction rate  $k$  is defined as:

$$k = A \exp(-E/RT), \quad (5)$$

$w$  = amount of unreacted component,  $A$  = frequency or pre-exponential factor,  $E$  = activation energy,  $R$  = universal gas constant and  $T$  = temperature. EASY%R<sub>o</sub> requires the extent of the reaction  $F$  (transform ratio) to be computed using:

$$F = -\frac{w}{w_0} = 1 - \sum_i f_i \left[ \frac{w_i}{w_{0i}} \right], \quad (6)$$

**Table 3.** Stoichiometric factors and activation energies used in the EASY%R<sub>o</sub> model produced by Sweeney & Burnham (1990)

Stoichiometric factor ( $f_i$ )	Activation energy ( $E$ ) (kcal mole <sup>-1</sup> )
0.03	34
0.03	36
0.04	38
0.04	40
0.05	42
0.05	44
0.06	46
0.04	48
0.04	50
0.07	52
0.06	54
0.06	56
0.06	58
0.05	60
0.05	62
0.04	64
0.03	66
0.02	68
0.02	70
0.01	72

where  $w$  = amount of unreacted component,  $w_0$  = the initial concentration of the total reactant,  $w_{0i}$  = initial concentration for component  $i$  and  $f_i$  = weight for  $i_{th}$  reaction (stoichiometric factor – Table 3). The transform ratio  $F$  for vitrinite reflectance (or the extent of the reaction) can then be used to calculate the EASY%R<sub>o</sub> vitrinite reflectance value using:

$$\text{EASY}\%R_o = \exp(3.7F - 1.6), \quad (7)$$

where 3.7 and  $-1.6$  are scaling factors calculated in the original derivation of EASY%R<sub>o</sub> Sweeney & Burnham (1990). A comprehensive description of the EASY%R<sub>o</sub> model is given in Appendix I of Sweeney & Burnham (1990), while a detailed explanation of the application of EASY%R<sub>o</sub> to a similar subsurface setting as modelled in this analysis is provided by Fjeldskaar *et al.* (2008) in their Appendix B.

The sills were modelled separately, recording the temperature of every node for every timestep for the entire 60, 000 years of each model run (Fig. 7). This produces a temperature–time pathway for every node, which can be input into the EASY%R<sub>o</sub> model of Sweeney & Burnham (1990). This procedure, however, does not account for maturation as a result of burial (Fig. 8).

As the sills were intruded and modelled at a shallow depth (260 and 590 m for the upper and lower sills respectively – Tucholke *et al.*, 2004a), they are thus exposed to relatively low background temperatures and therefore would not produce a representative background %R<sub>o</sub> gradient irrespective of model run time. To account for ‘Background’ maturation, resulting from burial-related heating a vitrinite gradient is applied after calculation of the maturation due to the heat from the sills. The background, vitrinite reflectance gradient used is calculated by comparing the vitrinite reflectance data for ODP 210–1276 by Pross *et al.* (2007) with a compilation from 28 extensional basins (Allen & Allen, 2005) (Fig. 8). The data used by Allen & Allen (2005) show a range of surface intercepts between 0.2 and 0.4%R<sub>o</sub> and with a gradient of  $0.15 \pm 0.09\% R_o \text{ km}^{-1}$  for depths <4 km. We have used a surface intercept of 0.4 and a gradient of  $0.15\% R_o \text{ km}^{-1}$  in our models as the observed data for ODP 210–1276 of Pross *et al.* (2007) lie at the upper end of the values for its depth. This method has allowed us to apply a representative background %R<sub>o</sub> gradient that has been calibrated using the (albeit limited) observed %R<sub>o</sub> data of Pross *et al.* (2007) (Fig. 8).

Modelled %R<sub>o</sub> is calculated as the maximum of the modelled vitrinite reflectance due to magmatic heating and the vitrinite reflectance due to burial-related heating at every depth node within the model. This procedure produces an estimate of vitrinite reflectance profile for the whole of ODP 210–1276, incorporating both the background, burial-related maturation and the maturation effects of the sills.

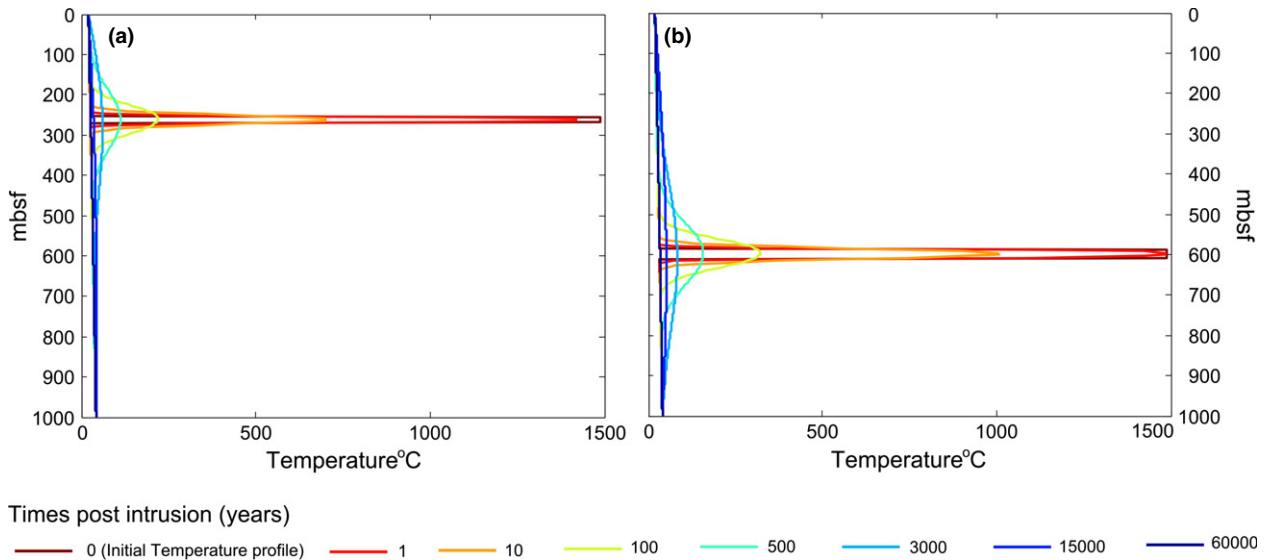


Fig. 7. 1D Thermal profiles for select times during the modelled cooling through from the upper (a) and lower sill (b) at ODP 210-1276. Time 0 depicts the initial temperature profile in each case, including the addition of the latent heat of crystallization. Modelling of the sills demonstrates that by 60,000 years the thermal anomaly created by the intrusion is virtually indistinguishable against the background geothermal gradient. The initial temperature conditions are shown as the time 0 years. Depth (m) is the depth at the time of intrusion according to the reconstruction by Tucholke *et al.* (2007).

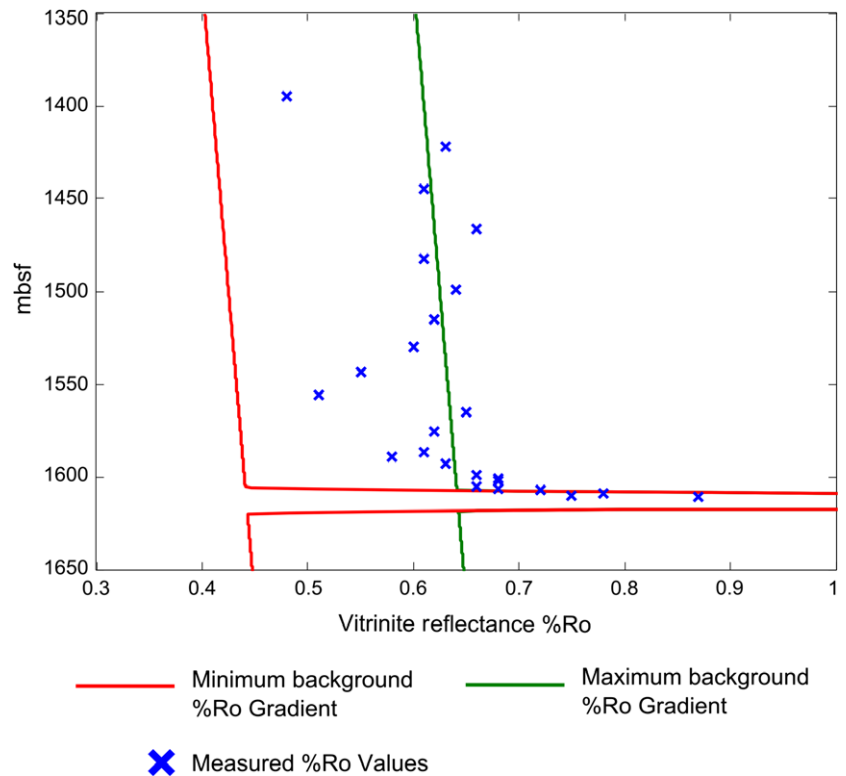
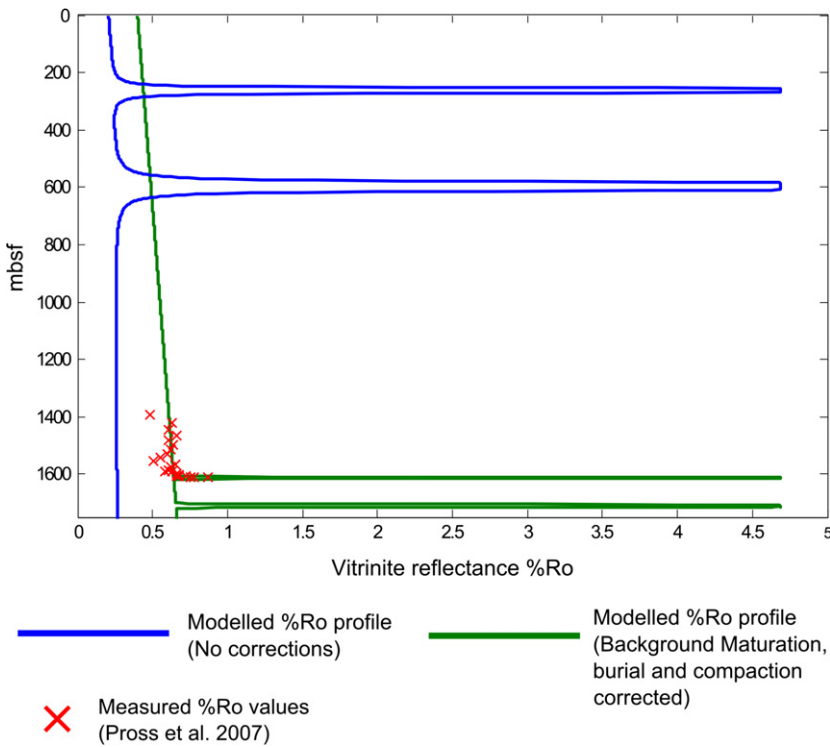


Fig. 8. Measured %Ro values (Pross *et al.*, 2007) alongside modelling results using both the minimum and maximum %Ro background values provided in Allen & Allen (2005). The data used by Allen & Allen (2005) are a compilation of data from 28 extensional basins, where the range of surface intercept is between 0.2 and 0.4%Ro and with a gradient of  $0.15 \pm 0.09\%Ro\ km^{-1}$  for depths <4 km. Both lines on this plot have a gradient of  $0.15\%Ro\ km^{-1}$ , with the ‘minimum’ using the surface intercept of 0.2%Ro and the ‘maximum’ using the surface intercept of 0.4%Ro.

### Burial and compaction

The sills were modelled at the estimated depths at the time of intrusion, as reconstructed from nano-fossil based age depth curves in Tucholke *et al.* (2004a). However, further burial and compaction of the sedimentary rocks occurred following intrusion. To allow accurate comparison

between the modelled and the observed vitrinite reflectance profiles (Fig. 9), we have therefore corrected the models for post-intrusion burial and compaction (Fig. 10). We assume that the sedimentary rocks underwent uniaxial compaction, but the thickness of the sills remains unchanged during burial. Post-intrusion compaction will have reduced the vertical extent of the thermal aureole.



**Fig. 9.** EASY%Ro vitrinite reflectance modelling (Sweeney & Burnham, 1990) results in proximity to both the upper and lower sills without any compensation for background maturation, compaction or burial (blue), alongside results corrected for background maturation, compaction and burial (green). This demonstrates the need to account for post-intrusion burial and compaction, and suggests that the spatial extent of the thermal influence upon maturation of these sills was much greater shortly after intrusion, but subsequent compaction has reduced the vertical extent of the aureole in the well.

Compaction is calculated by assuming uniform vertical shortening using the current vertical distance between the sills in the well by Tucholke *et al.* (2004a), and the reconstructed depths at the time of intrusion from Tucholke *et al.* (2007). This compaction factor was then applied uniformly to all sedimentary rocks at ODP 210-1276. This is reasonable as the rocks found between the sills are lithologically comparable to the relevant parts of the well (sections thermally influenced by the sills).

The position of the sills was corrected to account for burial again using the reconstructed depths at the time of intrusion of Tucholke *et al.* (2007) and the current depth in the well provided by Tucholke *et al.* (2004a). The burial correction was calculated from the top of the upper sill (in the well and the modelled depths). Both the compaction and burial corrections are schematically depicted in Fig. 10.

Compartmentalization of sedimentary basins by sill complexes is a well-known phenomenon (e.g. Holford *et al.*, 2012). It should therefore be noted that this compartmentalization will cause the degree of compaction sediments have undergone to be extremely variable. For this reason, our compaction correction is only applicable to the situation intersected at ODP 210-1276, and is unlikely to be representative of the entire area covered by the 'U-reflector'.

It can be shown that heating due to burial during the period of intrusive activity is negligible. If we consider the minimum and maximum ages of the upper and lower sills, by taking the mean  $^{40}\text{Ar}/^{39}\text{Ar}$  ages of Hart & Blusztajn (2006) (Fig. 3 and Table 1) and the minimum and maximum  $2\sigma$  uncertainties, it is likely that the shortest time between intrusion of the upper and lower sills was

1.5 Myrs and the longest time was 13.8 Myrs. Using the sedimentation rate of *ca.*  $17.8 \text{ mMyr}^{-1}$  noted by Tucholke *et al.* (2004a) at *ca.* 100 Ma these durations translate to upper and lower limits on the amount of burial as 27 and 246 m respectively. Applying the upper limit scenario (i.e. 246 m of sedimentation) to the geothermal gradient used in the model would only translate to a temperature difference of 5.4 K ( $0.246 \text{ km} \times 22^\circ\text{C km}^{-1}$ ), and thus the effect of additional burial-related maturation on organic matter would be negligible. All plots showing the sills at their current depth have been corrected for compaction and burial. This is consistent with our approach of modelling intrusion of the upper and lower sills as distinct thermal events.

### Hydrothermal activity

Although not the primary focus of this study, the effects of hydrothermal activity were estimated by increasing the thermal diffusivity for 10 and 20 m either side of the upper intrusion by one order of magnitude (Fig. 11). Previous work by Polyansky *et al.* (2003) on hydrothermalism induced by mafic intrusions emplaced at depths of 300–400 m, indicates that the effects can be observed above an intrusion at a distance of up to 1.5 times the diameter of the intrusion, while beneath an intrusion it can be observed up to a distance that is similar to the width of the intrusion. The upper sill at ODP 210-1276 is 10.3 m thick, thus in our model, enhanced diffusivity aureoles of 10 and 20 m (Fig. 11) are used, as a 20 m maximum extent of hydrothermalism either side of the sill is greater than the maximum estimates provided by Polyansky *et al.* (2003). As a result, a 20 m maximum extent

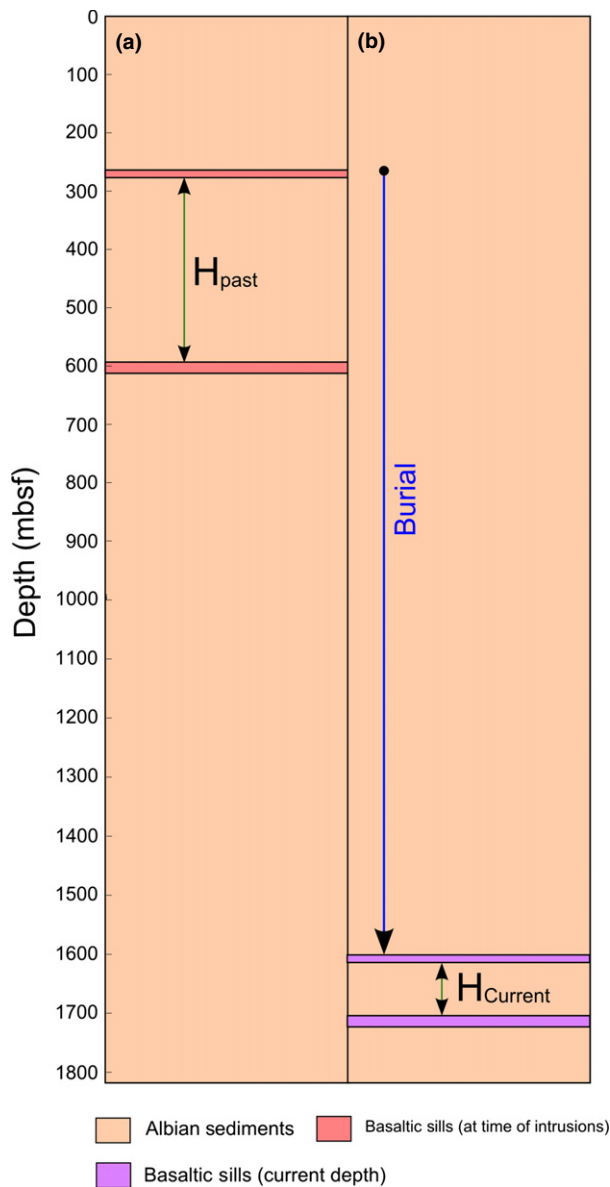


**Fig. 10.** A schematic depiction of the methodology used to account for sediment compaction and burial where; (a) is the reconstructed depths at time of intrusion and (b) represents the current depths recorded at ODP-210-1276. Compaction of the profile is calculated using the % difference between the measured current distance between the sills in the well ( $H_{\text{current}}$ ) and the reconstructed separation at the time of the intrusion ( $H_{\text{past}}$ ). This value was then taken to be the sediment compaction % for the whole profile. The sills are assumed to have remained the same thickness. Burial is measured in reference to the top of the upper sill, using the reconstructed value of 260 m and the current position in the well of 1612.7 m.

should overestimate the effects of hydrothermalism upon maturation, providing an end-member scenario.

Omission of advection is an assumption made by most workers in this field (e.g. Fjeldskaar *et al.*, 2008). This is probably the least reasonable of our assumptions as the effects of hydrothermal alteration have been observed in the well as subvertical calcite veins by Tucholke *et al.* (2004a) and potentially on seismic in

the form of disturbed Albian sedimentary rocks above the U-reflector by Peron-Pinvidic *et al.* (2010) at ODP 210-1276.

## RESULTS

The final model outputs are shown in Figs 6, 7, 11, 12, 13 and 14. Figures 12, 13 and 14 are depth and compaction corrected, whereas Figs 6, 7 and 11 are presented as the depth at time of sill intrusion.

Figure 6 depicts the maximum temperatures achieved from the models when the sills are intruded simultaneously alongside the results from the standard model, in which the sills are modelled separately. These results demonstrate that if simultaneous intrusion of multiple igneous bodies is assumed higher temperatures are achieved in proximity to the sills, particularly in the interval between the sills.

The temperature profiles for select times for the upper and lower intrusions are shown in Fig. 7. It can be seen that after approximately 15 000 years the thermal perturbation caused by the intrusions are virtually indistinguishable from the background geothermal gradient. As expected the thicker, lower sill takes longer to cool. The results demonstrate that the older sill had cooled to a value indistinguishable from the background geothermal gradient well before the second sill was intruded.

The results of the hydrothermal emulation models are presented in Fig. 11. It can be seen that even when the thermal diffusivity is increased by 1 order of magnitude for 20 m either side of the sill (Model 2 – the maximum hydrothermal influence modelled) the overall maximum temperature profile remains relatively unaffected and thus the influence upon maturation is also relatively insignificant as shown by the EASY% $R_o$  modelling results (Fig. 11).

The EASY% $R_o$  vitrinite reflectance results from the magmatic conduit duration experiments are provided in figure 12, along with the observed vitrinite reflectance values from Pross *et al.* (2007). These models show that in order to produce the observed vitrinite reflectance values above the upper sill, the duration in which the upper sill acted as a conduit probably was <10 years.

The maximum temperatures achieved from the intrusions, along with the current geothermal gradient (Keen, 1979) and TOC (wt%) (Tucholke *et al.*, 2004a) are shown on Fig. 13. These modelling results show that for a considerable portion of ODP 210-1276 the highest temperature achieved was due to the sill intrusion rather than subsequent burial. It can also be seen that if the oil/gas windows of England *et al.* (2002) are used (Fig. 13) the sedimentary rocks at ODP 210-1276 would not have been sufficiently heated to enter either the oil or gas windows without the additional heat from the sills.

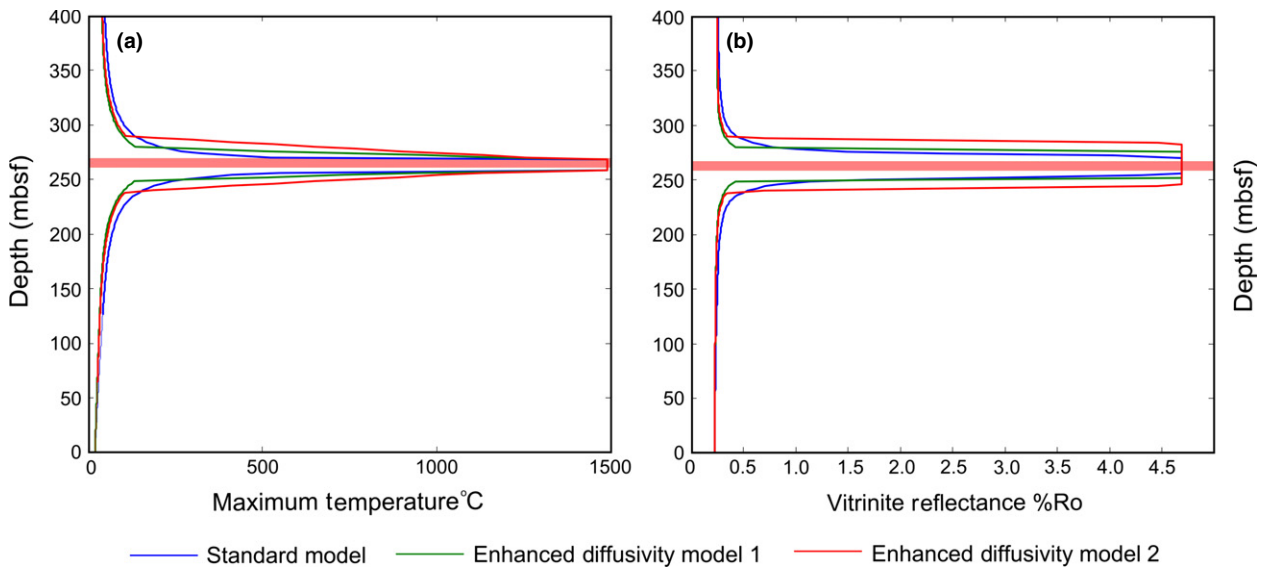


Fig. 11. Maximum temperatures (A) and EASY%Ro vitrinite reflectance modelling results (B) in proximity to the upper sill using both the standard modelling parameters outlined in the methodology and two models for ‘enhanced’ diffusivity to emulate the effects of hydrothermalism as a heat transfer mechanism. Model 1 represents increasing the diffusivity by one order of magnitude for 10 m either side of the sill, while Model 2 represents increasing diffusivity by 1 order of magnitude for 20 m either side of the sill.

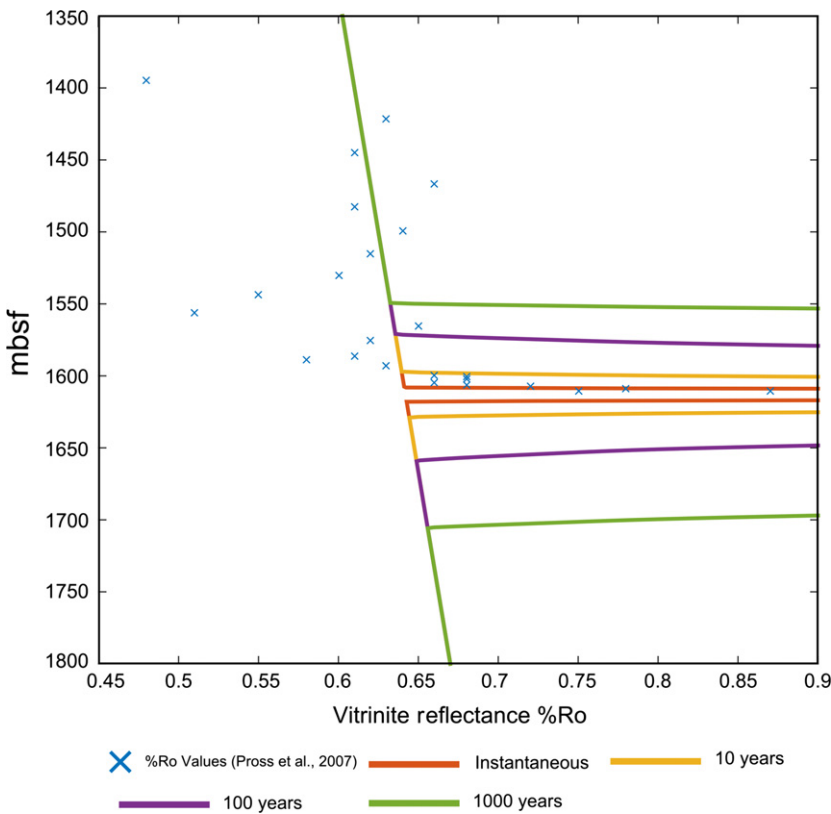


Fig. 12. EASY%Ro vitrinite reflectance modelling results (Sweeney & Burnham, 1990) produced by maintaining the starting temperature of the upper sill for 10, 100 and 1,000 years. This emulates the heating effects which would be caused by the upper sill remaining a magmatic conduit prior to the magma cooling to the closing temperature as recorded by the  $^{40}\text{Ar}/^{39}\text{Ar}$  ages.

The modelled vitrinite reflectance profile for the entirety of ODP 210–1276 is presented in Fig. 14. These results demonstrate that the sills have probably caused a vertically limited, yet significant deviation from the background vitrinite reflectance gradient produced from the data in Allen & Allen (2005).

## DISCUSSION

### Timing and duration of magmatism

Demonstrating that the older sill had cooled to a temperature indistinguishable from the estimated background

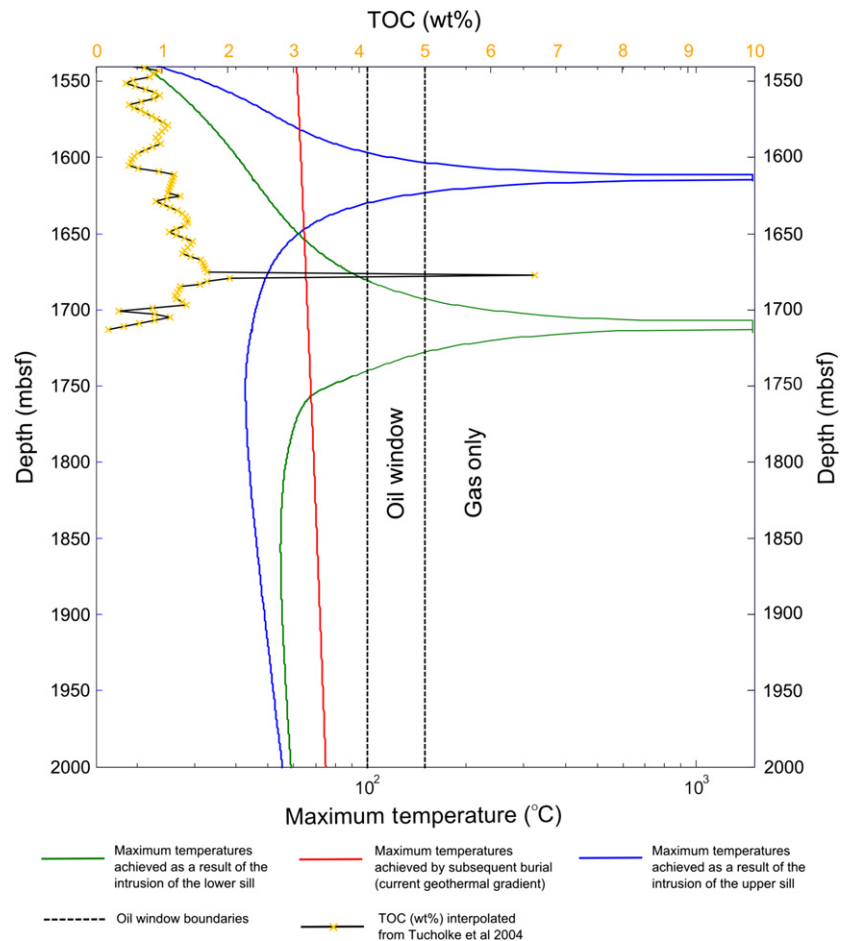


**Fig. 13.** The maximum temperatures achieved (logarithmic scale) as a result of sill intrusions and subsequent burial (current geothermal gradient – Keen, 1979), TOC (wt%) interpolated from the data in Tucholke *et al.* (2004a). This demonstrates that for a considerable portion of the well, the highest temperature achieved was due to heating from the intrusions rather than subsequent burial. This is assuming that the current burial depth is the maximum and that no exhumation has occurred. Oil and Gas windows from England *et al.* (2002).

geothermal gradient well before the second sill was intruded is significant. It shows that an assumption of simultaneous emplacement of multiple intrusive bodies (e.g. Aarnes *et al.*, 2010) could lead to an overestimation of the thermal perturbation. This has been demonstrated in Fig. 6 where it can be seen that if simultaneous intrusion of both sills is assumed, a higher maximum temperature is achieved in the region between the two sills. There is, however, no effect on the modelled vitrinite reflectance values, as the values generated for region between the sills (where there is greatest disparity in maximum temperature between the simultaneous and separate intrusion models – Fig. 6) are lower than the background vitrinite reflectance gradient from Allen & Allen (2005).

Our results indicate that, where possible, future models should avoid assuming simultaneous intrusion of multiple bodies, particularly in areas unlike ours where intrusions are shallow enough for the maturation effects not to be masked by subsequent burial-related maturation. When absolute dates are unavailable, other, nondirect methods can be used to estimate the duration of emplacement. One such method is to use the timing of forced folds above sills, such as the work by Magee *et al.* (2014) on the Irish Rockall Basin which indicates that emplacement took place during an interval of 15 Myrs. Where age constraints are not available as in this study, an end-member approach to modelling would be best. Using this approach

both a simultaneous intrusion model and a model whereby intrusions have cooled entirely before subsequent intrusions occur should be computed (Fig. 6).

Our models have demonstrated that the duration between the activation of the sill as a conduit and subsequent cooling to the closing temperature (as recorded by the  $^{40}\text{Ar}/^{39}\text{Ar}$  ages of Hart & Blusztajn, 2006) was probably  $<10$  years for the upper sill (Fig. 10). This implies that in order to produce such a widespread sill complex in a short duration of time, the system must have been fed from multiple points. It is also likely, that in addition, the sills intersected at ODP 210–1276 are not representative of the whole of the magmatic system imaged as the U-reflector. In order to achieve the magmatic flux required to produce such an apparently widespread sill complex, some parts of the system may have operated as conduits for longer prior to cooling than the sill modelled in this work.

Despite the upper sill not acting as a conduit for a prolonged period of time prior to cooling, the intrusion of these two compositionally similar upper and lower sills has occurred over a time span of *ca.* 10 Myrs (Hart & Blusztajn, 2006), thus a relatively long-lived, post-breakup mechanism is likely to have been required to produce the melt. Alternatively, the causal heat source may have diminished and been renewed on a timescale of *ca.*  $10^7$  years, although this seems less likely due to the similar composition of the two sills (Hart & Blusztajn, 2006).

The presence of a long-lived heat source could have influenced sediment maturation by introducing additional heat into the margin. This could explain the higher than average vitrinite reflectance gradient at this location on the margin (Fig. 8). Any elevated heat flow could have been caused by the same mechanism that generated the melts feeding the sills that are imaged on seismic data as the ‘U-reflector’ (Figs 1 and 2) and the two intrusions that are the subject of this modelling study.

### Implications for maturation

The modelled vitrinite reflectance profile for the entirety of ODP 210-1276 presented in Fig. 14 demonstrates that the sills have caused a vertically limited, yet significant spike in %R<sub>o</sub> that needs to be taken into account in source rock maturation studies. This is consistent with the vitrinite reflectance study by Pross *et al.* (2007), which notes thermal alteration associated with the upper sill is observable 20 m above the intrusion, with a

significant increase at 4.23 m and the highest value recorded closest to the sill at 2.17 m. Although the sills intersected at ODP 210-1276 may not be representative of the situation across the area covered by the U-reflector, if this high amplitude anomaly does indeed represent a widespread sill complex (e.g. Deemer *et al.*, 2010), then it is not unreasonable to suggest that a similar spike in maturation is likely to exist elsewhere on the Newfoundland margin where similar sills are present.

### Burial and compaction

Previous work proposes that the sills were intruded into relatively unconsolidated and not overpressured sedimentary rocks, particularly in the lower 30 m of the section (Tucholke *et al.*, 2007). It has been claimed that this suggests that at the drill site considerable mechanical support probably provided by nearby dykes, protecting the sedimentary rocks between the sills from compression (Peron-Pinvidic *et al.*, 2010).

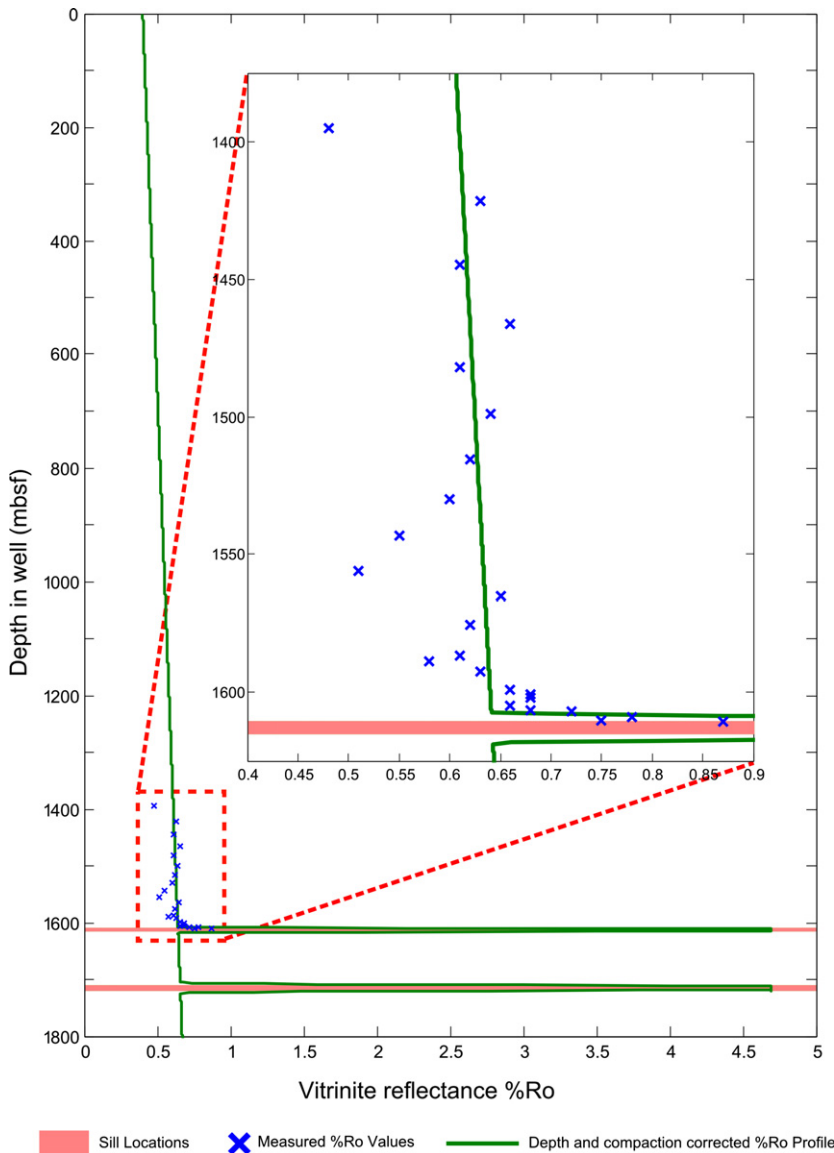


Fig. 14. Vitrinite reflection profile for the entirety of ODP 210-1276 produced using the EASY%Ro model of Sweeney & Burnham (1990) with the measured data provided by Pross *et al.* (2007) plotted alongside for comparison. It can be seen that a vertically limited, yet significant spike in %R<sub>o</sub> has been produced in proximity to the sills that needs to be taken into account in source rock maturation studies.

However, we find that the EASY%R<sub>o</sub> modelling results most closely resemble the observed vitrinite reflectance values when burial and compaction are accounted for (Fig. 8), perhaps suggesting that the sediments between the sills have been more compacted than previously suggested.

### Hydrothermal activity

Enhancing the diffusivity increases rate at which the sill cools, as expected, but has little effect on the modelled vitrinite reflectance values (Fig. 11). While these results are interesting, they demonstrate that the role of hydrothermalism, in this particular instance, is trivial in the context of the other assumptions and uncertainties inherent in the model and the parameters used. This implies that advection may not be as important in influencing maturation as suggested by previous work e.g. Polyansky *et al.* (2003).

### Source of the magmatism

The source of the magma producing the sills intersected at ODP210-1276, and probably of the U-reflector is still uncertain according to Peron-Pinvidic *et al.* (2010). It has been attributed to the migration of the Canary and Madeira plumes across the Newfoundland basin between 80 and 120 Ma (e.g. Karner & Shillington, 2005; Deemer *et al.*, 2010), which is said to be supported by the geochemical signature observed by Hart & Blusztajn (2006). Deemer *et al.* (2010) propose that volcanism was suppressed while the plumes travelled under the full thickness of the continental lithosphere, resulting in an accumulation of magma which was subsequently released when the hotspot approached the thinned lithosphere at the Eastern edge of the Grand Banks.

However, given that the Newfoundland Margin is considered to be a typical NVPM (e.g. Melankholina, 2011) with the absence of any other plume related observations, other causal mechanisms should be considered. One such alternative theory is proposed by Peron-Pinvidic *et al.* (2010) stating that the melts were produced by asymmetric rift-drift related tectono-magmatic processes.

## CONCLUSIONS

Collectively, the information acquired by the previous work at ODP 210-1276, and elsewhere on the Newfoundland Margin (e.g. Tucholke *et al.*, 2004a; Hart & Blusztajn, 2006; Pross *et al.*, 2007) has provided a unique opportunity to model the cooling of the sills and their thermal influence on the surrounding sedimentary rocks. This has allowed us to provide new insights into the relationship between intrusive magmatism, thermal evolution of passive margins and the influence on maturation on the

Newfoundland margin, within a well constrained framework. The key findings of this study include:

- (1) The oldest sill at ODP 210-1276 had cooled to a temperature indistinguishable from the background geothermal gradient well before the younger, lower sill complex was intruded.
- (2) The temperatures achieved in the sedimentary rocks adjacent to the intrusions are higher than those achieved by post-depositional burial. The sedimentary rocks at ODP 210-1276 would not have entered the oil or gas windows in the absence of this thermal pulse. This demonstrates the potential significance that regionally extensive intrusive magmatism could have on the thermal evolution of the Newfoundland margin, and suggests that the role of intrusive magmatism should be considered in thermal maturation studies in similar settings.
- (3) If the sills acted as magmatic conduits prior to cooling to the closing temperature (as recorded by the <sup>40</sup>Ar/<sup>39</sup>Ar dates) it was for a short duration, probably <10 years.
- (4) The peak in vitrinite reflectance data observed at ODP 210-1276 can be completely attributed to rapid heating from the upper sill. We have also shown that the spatial extent of the thermal aureole of these sills was much greater shortly after intrusion, and that subsequent burial and compaction has reduced its current vertical extent at ODP 210-1276, which is probably representative of the situation across the Newfoundland margin.
- (5) The higher than average %R<sub>o</sub> gradient for this part of the Newfoundland margin implies that at some point in the past the heat flow was elevated. This elevation of past heat flow could have been caused by the same mechanism that produced the sills which are imaged on seismic data as the 'U-reflector'.

Finally, the EASY%R<sub>o</sub> modelling results confirm that the sills at ODP 210-1276 have influenced the localized thermal evolution, and may be indicative of a broader, more regional thermal perturbation in the region covered by the 'U-reflector' on regional seismic data, and thus should be considered in source rock maturation studies.

## ACKNOWLEDGEMENTS

Funding for this research was provided by Royal Dutch Shell in the form of a CeREES studentship at Durham University. We also thank Jerry Sweeney and Alan Burnham for providing the EASY%R<sub>o</sub> model and guiding its application to our study. This research was made possible by data collected during leg 210 of the Ocean Drilling Program along with that collected during the SCREECH geophysical surveys. We thank Craig Magee and Nick Schofield for their constructive reviews which contributed significantly to this manuscript.

## REFERENCES

- AARNES, I., SVENSEN, H., CONNOLLY, J.A.D. & PODLADCHIKOV, Y.Y. (2010) How contact metamorphism can trigger global climate changes: modeling gas generation around igneous sills in sedimentary basins. *Geochim. Cosmochim. Acta*, **74**, 7179–7195.
- ALLEN, P.A. & ALLEN, J.R. (2005) *Basin Analysis*. Blackwell Publishing, Malden, MA, USA.
- BARKER, C.E., BONE, Y. & LEWAN, M.D. (1998) Fluid inclusion and vitrinite-reflectance geothermometry compared to heat-flow models of maximum paleotemperature next to dikes, western onshore Gippsland Basin, Australia. *Int. J. Coal Geol.*, **37**, 73–111.
- B EGLINGER, S.E., DOUST, H. & CLOETINGH, S. (2012) Relating petroleum system and play development to basin evolution: West African South Atlantic Basins. *Mar. Pet. Geol.*, **30**, 1–25.
- BOSTICK, N.H. & ALPERN, B. (1977) Principles of sampling, preparation and constituent selection for microphotometry in measurement of maturation of sedimentary organic matter. *J. Microsc.*, **109**, 41–47.
- BURNHAM, A.K. & SWEENEY, J.J. (1989) A chemical kinetic model of vitrinite maturation and reflectance. *Geochim. Cosmochim. Acta*, **53**, 2649–2657.
- DEEMER, S., HURICH, C. & HALL, J. (2010) Post-rift flood-basalt-like volcanism on the Newfoundland Basin nonvolcanic margin: the U event mapped with spectral decomposition. *Tectonophysics*, **494**, 1–16.
- DESILVA, N.R. (1999) Sedimentary basins and petroleum systems offshore Newfoundland and Labrador. *Geol. Soc. Lond. Petrol. Geol. Conf. Ser.*, **5**, 501–515.
- ELDHOLM, O. & SUNDVOR, E. (1979) Geological events during the early formation of a passive margin. *Tectonophysics*, **59**, 233–237.
- ENGLAND, G.L., RASMUSSEN, B., KRAPEZ, B. & GROVES, D.I. (2002) Archaean oil migration in the Witwatersrand Basin of South Africa. *J. Geol. Soc.*, **159**, 189–201.
- FJELDSKAAR, W., HELSET, H.M., JOHANSEN, H., GRUNNALEITE, I. & HORSTAD, I. (2008) Thermal modelling of magmatic intrusions in the Gjallar Ridge, Norwegian Sea: implications for vitrinite reflectance and hydrocarbon maturation. *Basin Res.*, **20**, 143–159.
- FRANKE, D. (2013) Rifting, lithosphere breakup and volcanism: comparison of magma-poor and volcanic rifted margins. *Mar. Pet. Geol.*, **43**, 63–87.
- GALUSHKIN, Y.I. (1997) Thermal effects of igneous intrusions on maturity of organic matter: a possible mechanism of intrusion. *Org. Geochem.*, **26**, 645–658.
- GEOFFROY, L. (2005) Volcanic passive margins. *C.R. Geosci.*, **337**, 1395–1408.
- GOUTORBE, B., DRAB, L., LOUBET, N. & LUCAZEAU, F. (2007) Heat flow of the Eastern Canadian rifted continental margin revisited. *Terra Nova*, **19**, 381–386.
- HART, S.R. & BLUSZTAJN, J. (2006) Age and geochemistry of the mafic sills, ODP Site 1276, Newfoundland margin. *Chem. Geol.*, **235**, 222–237.
- HEROUX, Y., CHAGNON, A. & BERTRAND, R. (1979) Compilation and correlation of major thermal maturation indicators. *AAPG Bull.*, **63**, 2128–2144.
- HOLFORD, S.P., SCHOFIELD, N., MACDONALD, J.D., DUDDY, I.R. & GREEN, P.F. (2012) Seismic analysis of igneous systems in sedimentary basins and their impacts on hydrocarbon prospectivity: examples from the Southern Australian margin. *APPEA J.*, **52**, 229–252.
- HOLFORD, S.P., SCHOFIELD, N., JACKSON, C.A.-L., MAGEE, C., GREEN, P.F. & DUDDY, I.R. (2013) Impacts of Igneous Intrusions on Source and Reservoir Potential in Prospective Sedimentary Basins Along the Western Australian Continental Margin. *West Australian Basins Symposium 18–21 August 2013*.
- HOPPER, J.R., FUNCK, T., TUCHOLKE, B.E., LARSEN, H.C., HOLBROOK, W.S., LOUDEN, K.E., SHILLINGTON, D. & LAU, H. (2004) Continental breakup and the onset of ultra-slow spreading off Flemish cap on the Newfoundland rifted margin. *Geology*, **32**, 93–96.
- KARNER, G.D. & SHILLINGTON, D.J. (2005) Basalt sills of the U reflector, Newfoundland basin: a serendipitous dating technique. *Geology*, **33**, 985–988.
- KEEN, C.E. (1979) Thermal history and subsidence of rifted continental margins—evidence from wells on the Nova Scotian and Labrador Shelves. *Can. J. Earth Sci.*, **16**, 505–522.
- MAGEE, C., JACKSON, C.A.L. & SCHOFIELD, N. (2014) Diachronous sub-volcanic intrusion along deep-water margins: insights from the Irish Rockall Basin. *Basin Res.*, **26**, 85–105.
- MELANKHOLINA, E.N. (2011) Passive margins of the North and Central Atlantic: a comparative study. *Geotectonics*, **45**, 291–301.
- PERON-PINVIDIC, G., SHILLINGTON, D.J. & TUCHOLKE, B.E. (2010) Characterization of sills associated with the U reflection on the Newfoundland margin: evidence for widespread early post-rift magmatism on a magma-poor rifted margin. *Geophys. J. Int.*, **182**, 113–136.
- PERON-PINVIDIC, G., MANATSCHAL, G. & OSMUNDSEN, P.T. (2013) Structural comparison of archetypal Atlantic rifted margins: a review of observations and concepts. *Mar. Pet. Geol.*, **43**, 21–47.
- POLYANSKY, O.P., REVERDATTO, V.V., KHOMENKO, A.V. & KUZNETSOVA, E.N. (2003) Modeling of fluid flow and heat transfer induced by basaltic near-surface magmatism in the Lena-Tunguska Petroleum Basin (Eastern Siberia, Russia). *J. Geochem. Explor.*, **78–79**, 687–692.
- PROSS, J., PLETSCH, T., SHILLINGTON, D.J., LIGOUIS, B., SCHELLENBERG, F. & KUS, J. (2007) Thermal alteration of terrestrial palynomorphs in mid-cretaceous organic-rich mudstones intruded by an igneous sill (Newfoundland Margin, ODP Hole 1276a). *Int. J. Coal Geol.*, **70**, 277–291.
- SHILLINGTON, D.J., HOLBROOK, W.S., TUCHOLKE, B.E., HOPPER, J.R., LOUDEN, K.E., LARSEN, H.C., VAN AVENDONK, H.J.A., DEEMER, S. & HALL, J. (2004) 5. Data Report: Marine Geophysical Data on the Newfoundland Nonvolcanic Rifted Margin around Screech Transect 2. *Proceedings of the Ocean Drilling Program, Initial Reports*, **210**, 1–36.
- SMITH, W.H.F. & SANDWELL, D.T. (1997) Global seafloor topography from satellite altimetry and ship depth soundings. *Science*, **277**, 1957–1962.
- SPEAR, F.S. & PEACOCK, S.M. (1989) *Metamorphic Pressure-Temperature-Time Paths*. American Geophysical Union, Washington, DC.
- SWEENEY, J.J. & BURNHAM, A.K. (1990) Evaluation of a simple model of vitrinite reflectance based on chemical kinetics. *AAPG Bull.*, **74**, 1559–1570.
- TUCHOLKE, B.E., SIBUET, J.-C. & KLAUS, A. (2004a) 1. Leg 210 Summary. *Proc. Ocean Drill. Program, Initial Rep.*, **210**, 1–78.
- TUCHOLKE, B.E., SIBUET, J.-C. & KLAUS, A. (2004b) 3. Site 1276. *Proc. Ocean Drill. Program, Initial Rep.*, **210**, 1–358.

- TUCHOLKE, B.E., SIBUET, J.-C. & KLAUS, A. (2007) 1. Leg 210 synthesis: tectonic, magmatic, and sedimentary evolution of the Newfoundland-Iberia rift. *Proc. ODP Sci. Results*, **210**, 1–56.
- VAN AVENDONK, H.J.A., HOLBROOK, W.S., NUNES, G.T., SHILLINGTON, D.J., TUCHOLKE, B.E., LOUDEN, K.E., LARSEN, H.C. & HOPPER, J.R. (2006) Seismic velocity structure of the rifted margin of the Eastern Grand Banks of Newfoundland, Canada. *J. Geophys. Res. Solid Earth*, **111**, B11404.
- WANG, D., LU, X., ZHANG, X., XU, S., HU, W. & WANG, L. (2007) Heat-model analysis of wall rocks below a diabase sill in Huimin Sag, China Compared with thermal alteration of mudstone to carbargilite and hornfels and with increase of vitrinite reflectance. *Geophys. Res. Lett.*, **34**, L16312.
- WANG, D., LU, X., SONG, Y., SHAO, R. & QI, T. (2010) Influence of the temperature dependence of thermal parameters of heat conduction models on the reconstruction of thermal history of igneous-intrusion-bearing basins. *Comput. Geosci.*, **36**, 1339–1344.
- WANG, K., LU, X., CHEN, M., MA, Y., LIU, K., LIU, L., LI, X. & HU, W. (2012) Numerical modelling of the hydrocarbon generation of tertiary source rocks intruded by doleritic sills in the Zhanhua depression, Bohai Bay Basin, China. *Basin Res.*, **24**, 234–247.

*Manuscript received 1 October 2014; In revised form 5 March 2015; Manuscript accepted 31 March 2015.*